A Predictive Physical Model for Hot-Carrier Degradation in Ultra-Scaled MOSFETs

Stanislav Tyaginov*,•, Markus Bina*, Jacopo Franco°, Yannick Wimmer*, Dmitri Osintsev*,
Ben Kaczer°, and Tibor Grasser*
*Institute for Microelectronics, Technische Universität Wien, 1040 Vienna, Austria
•A.F. Ioffe Physical-Technical Institute, 194021 Saint-Petersburg, Russia
°imec, Kapeldreef 75, B-3001 Leuven, Belgium
Email: tyaginov@iue.tuwien.ac.at

***Abstract*—We present and validate a novel physics-based model for hot-carrier degradation. The model incorporates such essential ingredients as a superposition of the multivibrational bond dissociation process and single-carrier mechanism, dispersion of the bond-breakage energy, interaction of the electric field and the dipole moment of the bond, and electron-electron scattering. The main requirement is that the model has to be able to cover HCD observed in a family of MOSFETs of identical architecture but with different gate lengths under diverse stress conditions using a unique set of parameters.**

I. Introduction

It has recently been understood that adequate physics-based modeling of hot-carrier degradation (HCD) requires a thorough treatment of carrier transport [1–4]. The population of hot carriers in the particle ensemble determines which of the competing Si-H bond-breakage mechanisms is dominant. In fact, in long-channel devices operating at higher voltages, these hot carriers are present in substantial numbers. Therefore, a solitary hot carrier can rapture a bond in a single collision, and thus trigger a so-called single-carrier process [4–7]. The bond dissociation is unlikely to occur in a direct collision of the hot electron with the hydrogen nucleus because the disparity between their masses is huge and only a negligible portion of energy is thus transfered to the proton [5]. Instead, it is assumed that such a hot carrier can excite one of the bonding electrons to an antibonding (AB) state, thereby making the bond unstable, see Fig. 1. Therefore, this single-carrier process is referred as the AB-process. Vice versa, in scaled devices subjected to hot-carrier stress under low voltages hot carriers are rare. Instead, the bond can be broken by a series of collisions with colder carriers. This multiple-carrier process leads to the multiple vibrational excitation (MVE) of the bond, which is termed the "MVE-process" [4–6, 8], see Fig. 1.

The rates of these mechanisms are very sensitive to the shape of the carrier energy distribution function (DF), which is, in turn, controlled by the scattering mechanisms. Among these mechanisms, electron-electron scattering (EES) is of particular importance for ultra-scaled devices. EES is suggested to be responsible for severe HCD enhancement in MOSFETs with channel lengths shorter than 70-100 nm [9]. Therefore, a proper HCD description needs to be based on a thorough carrier transport treatment. In most of the available physics-based models, however, single- and multiple-carrier bond-breakage processes as well as scattering mechanisms are assumed to be independent [10, 11].

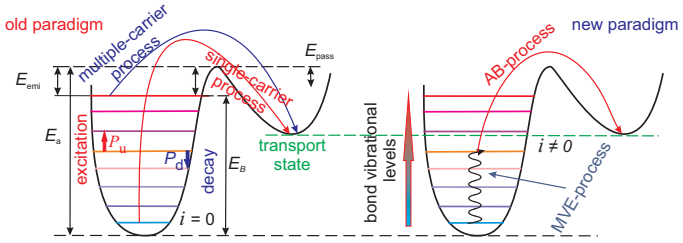

Fig. 1. A schematic representation of the bond dissociation process and the bond energetics. In previous HCD models only two limiting cases of bond rupture due to so-called single- and multiple-carrier processes were considered (left panel). Our model takes all possible combinations of bond heating via the MVE-process followed by the AB-mechanism and hydrogen release into account.

We present a physics-based model of HCD which is implemented in the deterministic Boltzmann transport equation solver ViennaSHE, see Fig. 2 [12, 13]. The model considers the AB- and MVE-processes as competing pathways of the same bond dissociation reaction, Fig. 1. The rates of such processes are controlled by the carrier DF, which is obtained with ViennaSHE. As the essential model ingredients, we also incorporate EES, statistical variations in the activation energy of the bond dissociation and its reduction induced by the interaction of the electric field with the bond dipole moment.

II. Experiment

We employ SiON nMOSFETs of the same architecture but with different gate lengths: L_G = 65, 100, and 150 nm ($L_{ch} \simeq$ 45, 80, and 120 nm). A 2.5 nm SiON gate dielectric was grown using decoupled plasma nitridation followed by the post-nitridation annealing. The devices were subjected to hot-carrier stress at the HCD worst-case conditions for two different V_{ds} = 1.8 and 2.2 V. Note that the worst-case conditions of HCD in a short-channel MOSFET correspond to $V_{gs} = V_{ds}$ [4, 9]. This is the case for the device with L_G = 65 nm. The MOSFET with L_G = 150 nm is treated as a long-channel transistor in terms of HCD [4, 9]. Also, the substrate current I_{sub} measured as a function of V_{gs} at a fixed V_{ds} has a maximum at $V_{gs} = V_{ds}/2$. $I_{sub}(V_{ds}, V_{gs})$ was also recorded for the 100 nm device resulting in a I_{sub} maximum at $V_{gs} = 2/3V_{ds}$. Thus, we stressed the MOSFETs with L_G = 65, 100, and 150 nm at $V_{gs} = V_{ds}$, $V_{gs} = 2/3V_{ds}$, and $V_{gs} = 1/2V_{ds}$, respectively at T = 298 K.

978-1-4799-5288-5/14/$31.00 © 2014 IEEE

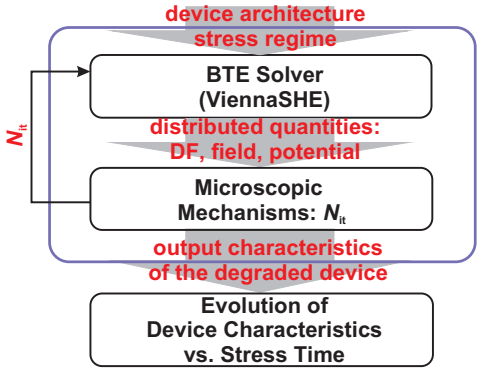

Fig. 2. Our physics-based HCD model includes three main subtasks, which are implemented into the Boltzmann transport equation solver ViennaSHE: a carrier transport treatment, microscopic mechanisms of defect generation, and modeling of the degraded devices.

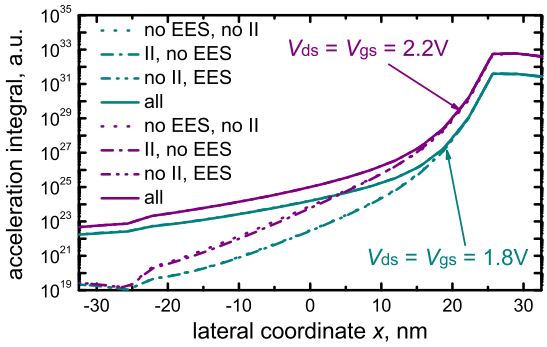

Fig. 4. The carrier acceleration integrals are plotted for the 65 nm device stressed at V_{gs} = V_{ds} = 1.8 V and 2.2 V with and without the effects of EES and impact ionization. Since EES populates the high-energy tail of the DFs the carrier AIs substantially change due to this mechanism, while impact ionization has almost no effect.

III. The Model

Our physics-based model incorporates three main submodules: a transport module, the description of microscopic mechanisms of defect generation, and the simulations of the degraded devices [4, 13], see Fig. 2. The transport module is realized on the basis of ViennaSHE, which calculates carrier DFs for a given device topology and specified stress conditions. The device architecture is obtained using the Sentaurus Process simulator. Since DFs are very sensitive to the doping profiles, the process and device simulators are coupled and thoroughly calibrated in order to represent IV characteristics of the fresh MOSFETs. A family of non-equilibrium carrier DFs calculated for the 65 nm device with and without electron-electron scattering for V_{gs} = V_{ds} = 2.2 V is plotted in Fig. 3. One can see that EES substantially changes the DF shape by populating the high-energy tails. This effect is more pronounced near the drain. At the source, the DFs demonstrate a Maxwellian rudiment, while in the center of the device and in the drain area they are severely non-equilibrium. This results e.g. in a plateau visible at moderate energies. The DFs are

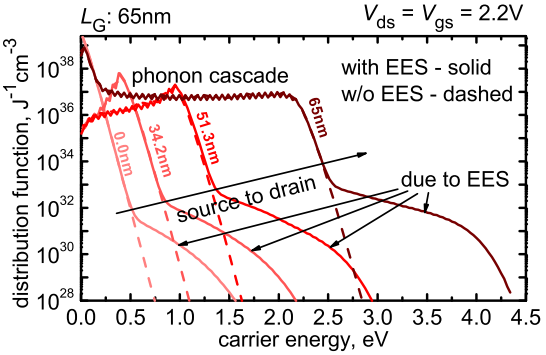

Fig. 3. The distribution functions for the 65 nm device stressed at V_{gs} = V_{ds} = 2.2 V considering and ignoring EES. One can see that EES substantially changes the shape of the high-energy tail of the DFs.

then used to calculate the carrier acceleration integral (AI) [4, 5, 14–16] (see Fig. 4). The carrier AI represents the cumulative ability of the carrier ensemble to dissociate the Si-H bonds, and thus determines the rates of both AB- and MVE-mechanisms. It is evaluated as a product of the carrier flux in the elementary energy range of $[E; E + \mathrm{d}E]$ which impinges on the bond the energy-dependent reaction cross section; this product is then integrated over the hole energy range:

$$I_{\mathrm{ab/mve}}^{(\mathrm{e/h})} = \int_{E_{\mathrm{th}}}^{\infty} f^{(\mathrm{e/h})}(E) g^{(\mathrm{e/h})}(E) \sigma_{\mathrm{ab/mve}}^{(\mathrm{e/h})}(E) v(E) dE, \quad (1)$$

where $f^{(\mathrm{e/h})}(E)$ is the DFs for electrons/holes, $g^{(\mathrm{e/h})}(E)$ the corresponding density-of-states, $\sigma_{\mathrm{ab/mve}}(E)$ the reaction cross section, while $v(E)$ the group velocity. It it is important to emphasize that we describe the *AB- and MVE-mechanisms as competing pathways* of the same reaction which converts neutral precursors (passivated Si-H bonds) to the charged defects ($\mathrm{P_b}$ centers). In other words, we *consider all the superpositions of these mechanisms* when first the bond can be heated to a certain intermediate level i by a series of colder electrons and then bombarded by a high energetical carrier which triggers an AB-mechanism, see Fig. 1, right panel. Note that hydrogen release from the intermediate level i occurs over the reduced potential barrier of the height $E_{\mathrm{a}} - E_i$, where E_{a} is the bond dissociation energy and E_i the energetical position of the level. In (1) the Keldysh-like reaction cross section is $\sigma_{\mathrm{ab/mve}}^{(\mathrm{e/h})}(E) = \sigma_{0,\mathrm{ab/mve}}^{(\mathrm{e/h})}(E - E_{\mathrm{th,ab/mve}})^{p_{\mathrm{it}}}$. The threshold energy $E_{\mathrm{th,ab}}$ in the case of the AB-process just corresponds to the barrier height $E_{\mathrm{a}} - E_i - d \times E_{\mathrm{ox}}$. The term $d \times E_{\mathrm{ox}}$ describes the interaction of the oxide electric field with the dipole moment of the bond, which reduces the bond-breakage energy [7]. As for the MVE-process, we consider the Si-H bond as a truncated harmonic oscillator [4, 5, 7] (see Fig. 1) and $E_{\mathrm{th,mve}}$ is equal to the distance between the oscillator levels $\hbar\omega$.

To summarize, the acceleration integral for the AB-process from the level i is:

$$I_{\mathrm{ab},i} = \int f(E) g(E) \sigma_0 (E - E_{\mathrm{a}} + E_i + d \times E_{\mathrm{ox}})^{p_{\mathrm{it}}} v(E) \mathrm{d}E. \quad (2)$$

The corresponding rate is calculated as a superposition of the Arrhenius term which corresponds to the thermal activation of the proton over the potential barrier and the acceleration integral which represents the effect of hot carriers:

$$R_{\mathrm{ab},i} = w_{\mathrm{th}} \exp\left[-\left(E_{\mathrm{a}} - E_i\right)/k_{\mathrm{B}}T\right] + I_{\mathrm{AB},i}. \quad (3)$$

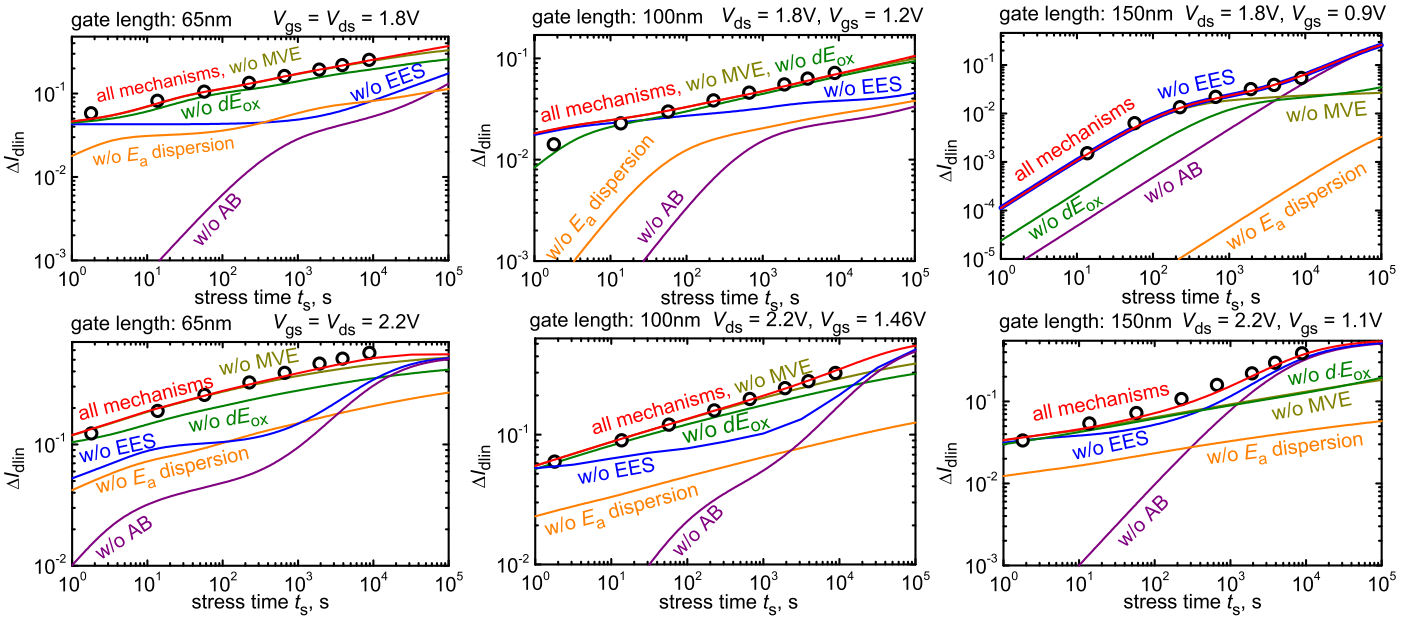

Fig. 5. The relative change of linear drain current $\Delta I_{\rm dlin}$ as a function of stress time: experiment (symbols) vs. simulations (lines) plotted for three different MOSFETs with $L_{\rm G}$ = 65, 100, and 150 nm. Devices were stressed at worst-case conditions at $V_{\rm ds}$ = 1.8 and 2.2 V. The curves obtained neglecting one of the model ingredients are plotted for comparison. EES plays an important role for $L_{\rm G}$ = 65 and 100 nm, being substantially less significant for $L_{\rm G}$ =150 nm even at high $V_{\rm ds}$.

In the case of the MVE-process the corresponding AI enters the bond excitation/deexcication rates:

$$\begin{aligned} P_{\rm u} &= \omega_{\rm e}\exp\left(-\hbar\omega/k_{\rm B}T_{\rm L}\right) + I_{\rm MVE}, \\ P_{\rm d} &= \omega_{\rm e} + I_{\rm MVE} \end{aligned} \tag{4}$$

with $\omega_{\rm e}$ being the reciprocal phonon life-time.

The bond-breakage kinetics is described by the system of rate equations:

$$\begin{aligned} \frac{{\rm d}n_0}{{\rm d}t} &= P_{\rm d}n_1 - P_{\rm u}n_0 - R_{{\rm a},0}n_0 + R_{{\rm p},0}N_{\rm it}^2 \\ \frac{{\rm d}n_i}{{\rm d}t} &= P_{\rm d}(n_{i+1} - n_i) - \\ &\quad -P_{\rm u}(n_i - n_{i-1}) - R_{{\rm a},i}n_i + R_{{\rm p},i}N_{\rm it}^2 \\ \frac{{\rm d}n_{N_l}}{{\rm d}t} &= P_{\rm u}n_{N_{l-1}} - P_{\rm d}n_{N_l} - R_{{\rm a},N_l}n_{N_l} + R_{{\rm p},N_l}N_{\rm it}^2, \end{aligned} \tag{5}$$

where N_l labels the last bonded state, n_i are the oscillator occupation numbers and rates $R_{\rm a/p,\it i}$ represent the rates of the depassivation/passivation processes. The system (5) is solved by taking into account a huge disparity between the characteristic times, which describe establishment of the oscillator steady-state, and those typical for bond-breakage and dissociation processes. As a result, the system reduces to a solitary equation:

$$\frac{{\rm d}N_{\rm it}}{{\rm d}t} = \left(N_0 - N_{\rm it}\right)\Re_{\rm a} - N_{\rm it}^2\Re_{\rm p}, \tag{6}$$

with N_0 being the concentration of pristine Si-H bonds and the cumulative bond-breakage rate calculated as:

$$\Re_{\rm a} = \frac{1}{k}\sum_i R_{{\rm a},i}\left(\frac{P_{\rm u}}{P_{\rm d}}\right)^i, \tag{7}$$

where k is is the normalization prefactor:

$$k = \sum_i \left(\frac{P_{\rm u}}{P_{\rm d}}\right)^i. \tag{8}$$

As for the cumulative passivation rate $\mathfrak{P} = \sum_i P_i$ without loss of generality one may represent the $\mathfrak{P}$ rate by the Arrhenius term for thermal activation over a single barrier, i.e.

$$\mathfrak{P} = \nu_{\rm p}\exp(-E_{\rm pass}/k_{\rm B}T_{\rm L}), \tag{9}$$

where $\nu_{\rm p}$ is the attempt rate.

The analytic solution of (6) is:

$$\begin{aligned} N_{\rm it}(t) &= \frac{\sqrt{\Re_{\rm a}^2/4 + N_0\Re_{\rm a}\Re_{\rm p}}}{\Re_{\rm p}}\frac{1-f(t)}{1+f(t)} - \frac{\Re_{\rm a}}{2\Re_{\rm p}}, \\ f(t) &= \frac{\sqrt{\Re_{\rm a}^2/4 + N_0\Re_{\rm a}\Re_{\rm p}} - \Re_{\rm a}/2}{\sqrt{\Re_{\rm a}^2/4 + N_0\Re_{\rm a}\Re_{\rm p}} + \Re_{\rm a}/2}\times \\ &\quad \times\exp\left(-2t\sqrt{\Re_{\rm a}^2/4 + N_0\Re_{\rm a}\Re_{\rm p}}\right). \end{aligned} \tag{10}$$

Note finally that the bond-breakage activation energy varies statistically. This is related to the amorphous nature of the SiON films and disorder at the Si/SiON interface. The activation energy dispersion is modeled using a Gaussian distribution with $\langle E_{\rm a}\rangle$ = 1.5 eV and $\sigma_{\rm E}$ = 0.15 eV. These values are in agreement with experimental ones [17, 18].

IV. Results and Discussion

The model was validated against the experimental dependences of the linear drain current change vs. stress time $\Delta I_{\rm dlin}(t)$. Fig. 5 reveals good agreement between experimental and simulation results. *Our physics-based model* is capable of representing $\Delta I_{\rm dlin}(t)$ curves for different devices and under

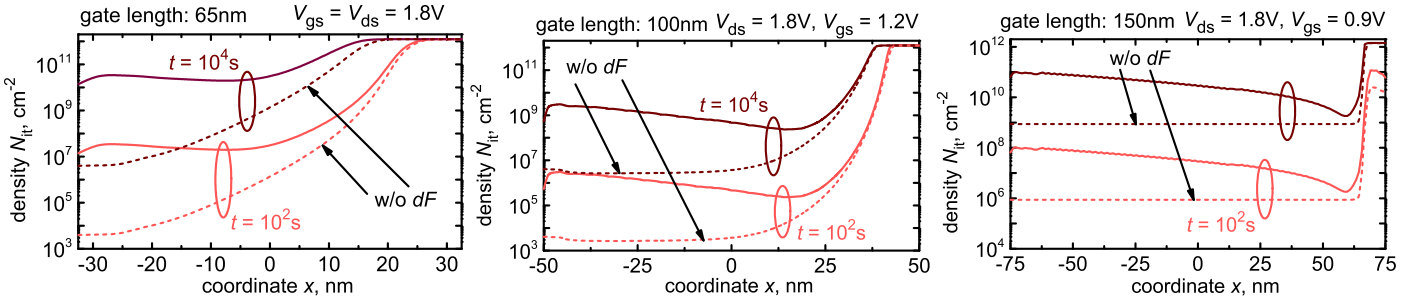

Fig. 6. The interface trap concentration as a function of the lateral coordinate $N_{\rm it}(x)$ calculated with and without the lowering of the activation energy $d \times E_{\rm ox}$. These profiles are calculated for all three devices and for stress time of 10 s and 10ks. One can see that the interaction with the electric field leads to an increase of $N_{\rm it}$ near the source, while without this effect the concentration remains constant.

different stress conditions *using the same set of model parameters*. Fig. 5 summarizes $\Delta I_{\rm dlin}(t)$ plots calculated disregarding one of the model ingredients. If the AB-mechanism is deactivated, the discrepancy between experimental and simulated $\Delta I_{\rm dlin}(t)$ dependences is most pronounced at short stress times, tending to zero for long stresses. Ignoring EES has the same effect on the $\Delta I_{\rm dlin}(t)$ curves as suppression of the AB-mechanism. This is because EES populates the high energetical fraction of the carrier ensemble, and thus enforces the AB-process, cf. Fig. 3. In longer devices, the contribution of EES becomes less pronounced and almost negligible in the device with $L_{\rm G}$=150 nm even at high $V_{\rm ds}$ = 2.2 V.

One can see that the long-term degradation is determined by the $d \times E_{\rm ox}$ energy reduction, especially in long-channel devices. This trend is supported by $N_{\rm it}(x)$ profiles for all three devices stressed at $V_{\rm ds}$ = 1.8 V for 10 s and 10 ks considering and ignoring the $d \times E_{\rm ox}$ effect, Fig. 6. Such a bond weakening results in an increase of $N_{\rm it}$ near the source, which becomes more significant at longer stress times. Ignoring the bond-breakage energy dispersion massively shifts all $\Delta I_{\rm dlin}(t)$ curves towards lower values. It is quite intriguing that the importance of the MVE-mechanism becomes more substantial for MOSFETs with longer gate lengths. At a first glance this looks contradictory to the commonly adopted idea that the MVE-process, which determines HCD in ultra-scaled transistors, is less pronounced in longer counterparts [4, 6, 8]. In this study, however, we have intentionally chosen such stress conditions (at high voltages) that both AB- and MVE-processes are relevant. As a result, one cane see that even in the scaled MOSFET the former mechanism plays a crucial role. If, however, the drain voltage $V_{\rm ds}$ is fixed and the gate length increases, the high-energy tails of the DFs are less pronounced. As a result, the relative contribution of the AB-process decreases, while the MVE-process becomes more prominent. Therefore, the main message is that the *importance of AB/MVE-mechanisms* is not defined exclusively by the channel length but *is controlled by the combination of the device architecture and the applied voltages*.

V. Conclusion

We have presented and verified a physics-based model which represents HCD in a wide range of MOSFETs starting from scaled transistors with the gate length of 65 nm and ending at longer counterparts with $L_{\rm G}$ = 150 nm. The model uses a single set of parameters and can *be employed for predictive simulations*. Our approach incorporates important ingredients of HCD such as EES, superposition of the MVE- and AB-mechanisms, statistical variations of the bond-breakage energy and its reduction due to the interaction with the electric field. Note that the AB- and MVE-mechanisms of Si-H bond-breakage are considered self-consistently as competing pathways of the same dissociation reaction. We also have shown that in the scaled devices the role of EES is important, while the MVE-process and the interaction between the dipole moment of the bond determine long-term HCD.

Acknowledgment

The authors acknowledge support by the Austrian Science Fund (FWF), grants P23598 and P26382, and the European Community FP7 projects N$^{\rm o}$ 261868 (MORDRED) and 619246 (ATHENIS_3D).

References

[1] S. Reggiani *et al.*, in *Proc. European Solid-State Device Research Conference (ESSDERC)* (2012), pp. 185–188.

[2] Y. Randriamihaja *et al.*, in *Proc. International Reliability Physics Symposium (IRPS)* (2013), pp. 1–5.

[3] S. Tyaginov *et al.*, in *Proc. European Solid-State Device Research Conference (ESSDERC)* (2011), pp. 151–154.

[4] S. Tyaginov *et al.*, in *Proc. International Integrated Reliability Workshop (IIRW)* (2012), pp. 206–215.

[5] W. McMahon *et al.*, in *Proc. Int. Conf. Mod. Sim. Micro* (2002), Vol. 1, pp. 576–579.

[6] A. Bravaix *et al.*, in *Proc. European Symposium on Reliability of Electron Devices Failure Physics and Analysis (ESREF), tutorial* (2010).

[7] C. Guerin *et al.*, Journ. Appl. Phys. **105**, 114513 (2009).

[8] S. Rauch *et al.*, in *Proc. International Reliability Physics Symposium (IRPS), tutorial* (2010).

[9] S. Rauch *et al.*, IEEE Trans. Dev. Material. Reliab. **1**, 113 (2001).

[10] C. Guerin *et al.*, IEEE Trans. Dev. Material. Reliab. **7**, 225 (2007).

[11] Y. Randriamihaja *et al.*, Microel. Reliab. **52**, 2513 (2012).

[12] K. Rupp *et al.*, in *Proc. International Electron Devices Meeting (IEDM)* (2011), pp. 789–792.

[13] M. Bina *et al.*, in *Proc. International Electron Devices Meeting (IEDM)* (2012), pp. 713–716.

[14] K. Hess *et al.*, Physica E **3**, 1 (1998).

[15] S. Rauch *et al.*, IEEE Trans. Dev. Material. Reliab. **5**, 701 (2005).

[16] S. Tyaginov *et al.*, in *Proc. International Conference on Simulation of Semiconductor Processes and Devices (SISPAD)* (2011), pp. 123–126.

[17] A. Stesmans, Applied Physics Letters **68**, 2723 (1996).

[18] G. Pobegen *et al.*, IEEE Electron Dev. Lett. **34**, 939 (2013).